Hysteretic Behavior in an Fe-Cr-Ni-Mn-Si Polycrystalline Shape Memory Alloy During Thermomechanical Cyclic Loading

K. Tanaka, T. Hayashi, F. Nishimura, and H. Tobushi

Stress-strain-temperature hysteretic behavior is examined in an Fe-Cr-Ni-Mn-Si polycrystalline shape memory alloy during thermomechanical cyclic loading, each cycle of which consists of isothermal loading/unloading followed by isostatic heating/cooling. Transformation start and finish lines are first determined in the stress-temperature plane, which are revealed to be less cycle dependent. Hysteretic behavior is, on the contrary, shown to be highly cycle dependent. Its strong dependence on hold stress as well as on temperature range is also examined. The martensite start line is clearly determined above the yield stress of the parent phase.

Keywords

Fe-based shape memory alloy, hysteresis, thermomechanical cyclic loading

1. Introduction

THE Fe-base shape memory alloys have been studied extensively as the leading practical shape memory alloys following Ti-Ni alloys and Cu-base alloys. The shape memory effect, although only a one-way shape memory effect has been reported,[1-3] is observed in such ferrous alloys as stainless steels (SUS 304), iron/high-manganese alloys, Fe-Ni-Co-Ti alloys, Fe-Mn-Si alloys, and others.[4-9] The crystal structure of the martensite is bct α', or fct or cph ε in these alloys. In stainless steels and iron/high-manganese alloys, the effect is due solely to the reverse transformation of stress-induced ε martensite. Because the formation of the normal α' martensite accompanies a large volume expansion of about 5%, which inevitably induces local plastic deformation and results in less shape recovery, the alloys have been designed to either metallurgically decrease the volume expansion of α' martensite or to use the ε martensite, which accompanies very small volume expansion. Strengthening of the weak parent (austenite, γ) phase is another way to achieve a greater amount of shape recovery, because it retards plastic deformation at an early stage of loading.

The high strength of iron-base shape memory alloys, together with their low cost, strongly attracts the attention of designers of the shape memory devices because use of these alloys enables design of larger size devices. These devices are expected to play the role of the structural members in the structures, carrying the actual thermomechanical loads. To promote and to achieve this goal, the three-dimensional unified theory, which describes the thermomechanical/transformation behaviors in alloys, should be developed based on transformation thermomechanics. The code of the numerical analyses should also be prepared to solve the practical boundary/initial value problems for the mechanical (stress, strain, and displacement), thermal (temperature), and metallurgical (volume fraction of phases) quantities.

This scheme must be supported experimentally by obtaining accurate experimental data on these alloys. Some of the topics to be investigated from a macroscopic point of view include the transformation start and finish stresses and their temperature dependence; stress-strain-temperature relation; recovery stress during heating; full and subloops under isothermal, isostatic, or thermomechanical loading; and the cyclic effect on the hysteretic behavior. Metallurgical observations must, of course, be supplemented when the transformation kinetics is formulated or when the cyclic behavior is discussed.

In this article, the hysteretic behavior of a Fe-9Cr-5Ni-14Mn-6Si polycrystalline shape memory alloy was studied during thermomechanical loading. The alloy was developed as an advanced shape memory alloy by adjusting the chromium content to exhibit high corrosion resistance while still maintaining the high strength of iron-base alloys.[10,11] This alloy has improved oxidation resistance and workability compared to conventional nonferrous shape memory alloys. The mechanical performance of the alloy, stress-strain-temperature hysteresis, and its cycle dependence is presented from a macroscopic point of view to provide the data for establishing the unified transformation/thermomechanical theory.

2. Alloy, Experimental Apparatus, and Experimental Procedure

The alloy tested in the present study was prepared by vacuum induction melting.[10,11] The chemical composition and the mechanical properties of the alloys at room temperature (RT, 303 K) are given in Tables 1 and 2, respectively. After hot rolled plate was homogenized at 1323 K for 3.6 ks, 6-mm diam test specimens with 20 mm gage length (Fig. 1) were machined from the plate.

Tests were carried out with a servohydraulic thermal fatigue testing machine (Shimadzu, EHF-ED5/TD-5-10L) equipped with a high-frequency induction heater. Mechanical and thermal cyclic loading was applicable independently in any form of time history. Tensile displacement was measured with a differ-

K. Tanaka, T. Hayashi, and **F. Nishimura,** Department of Aerospace Engineering, Tokyo Metropolitan Institute of Technology, Hino/Tokyo, Japan; and **H. Tobushi,** Department of Mechanical Engineering, Aichi Institute of Technology, Toyota, Japan.

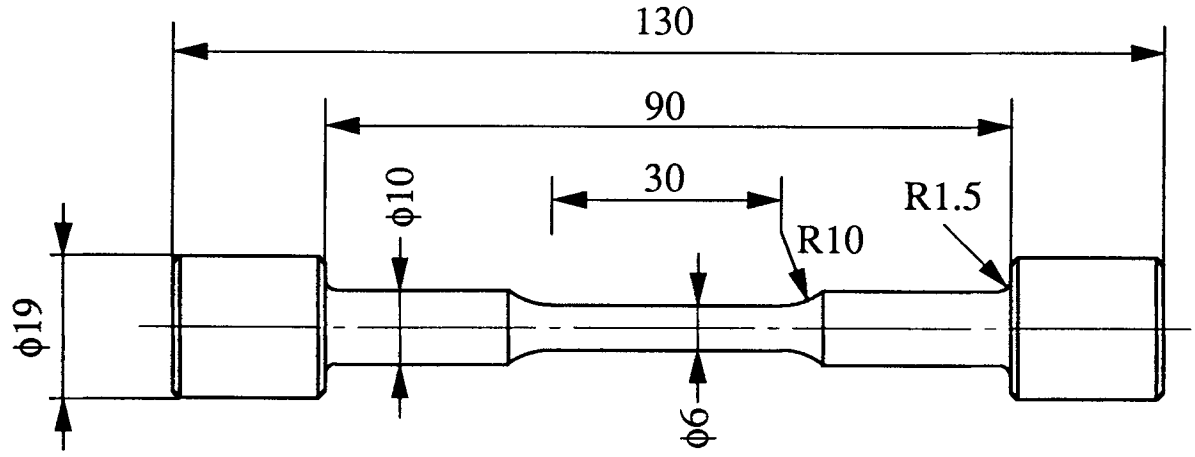

Fig. 1 Typical test specimen.

Table 1 Chemical composition of test alloy

Composition, wt%						
Cr	Ni	Mn	Si	C	N	Fe
9.0	5.2	14.4	6.0	0.02	0.005	Bal

Table 2 Mechanical properties at room temperature

0.2% proof stress ($\sigma_{0.2}$), MPa	Tensile strength (σ_f), MPa	Elongation (ϕ), %	Area contraction (ψ), %	Young's modulus (E), MPa
2.58×10^2	7.88×10^2	70.5	61.1	1.26×10^5

ential transformer, whereas the temperature of the specimen was detected with a platinum/platinum-rhodium thermocouple spotwelded at the center in the gage length. All experimental procedures were monitored and controlled by a personal computer (PC). The output data of the tests were stored in the PC memory for later analyses.

To obtain a stable thermomechanical state in the specimen, the following procedure was carried out four times successively prior to the tests.[10,11] First, the specimen was mechanically loaded to 4% at RT and was unloaded. Thermal heating to 873 K, holding for 600 s, and successive cooling to RT then followed.

Thermomechanical cyclic loading tests were performed along the path schematically illustrated in Fig. 2. Each thermomechanical cycle was composed of an isothermal mechanical branch, loading/unloading between the lower limit stress σ_h and the upper limit stress σ_{max} at a hold temperature T_h, and a subsequent isostatic thermal branch, heating/cooling between the lower limit temperature T_h and the upper limit temperature T_{max} under a hold stress σ_h. During the entire test, the loading and unloading rates were kept constant at about 3 MPa/s, and the heating rate was maintained at about 3 K/s. The cooling rate was also maintained at the same constant value by controlling the pressurized air flow to the specimen.

The martensite start stress, σ_{Ms}, was measured from the stress-strain output during the mechanical branch of cycling as the 0.2% proof stress, whereas the austenite start temperature, T_{As}, and the austenite finish temperature, T_{Af}, were determined from the strain-temperature output during the thermal branch of loading. The stress-induced martensitic transformation never reached completion during loading in this alloy. The martensite finish stress, σ_{Mf}, therefore, could not have been measured. The yield stress $\sigma_{0.2}$, or 0.2% proof stress, and the tensile strength, σ_f, exhibited a strong temperature dependence.

3. Transformation Lines

The transformation behavior of the alloy, as illustrated by transformation lines, is shown in Fig. 3 and 4. Because both the reverse transformation start and finish lines depend strongly on preloading, these figures show only the data obtained with the specimens preloaded to $\sigma_{max} = 350$ MPa prior to the heating/cooling thermal run. The transformation lines were found to be almost parallel in the temperature-stress plane, and their slope is about 2.17 MPa/K. A wide reverse transformation range, $T_{Af} - T_{As} \approx 180$ K, and a narrow elastic domain over almost the complete temperature range are the typical characteristics in this alloy. Pseudoelastic behavior, therefore, cannot be expected at any temperature. The thermomechanical loading illustrated in Fig. 2 is the only possible way to achieve the

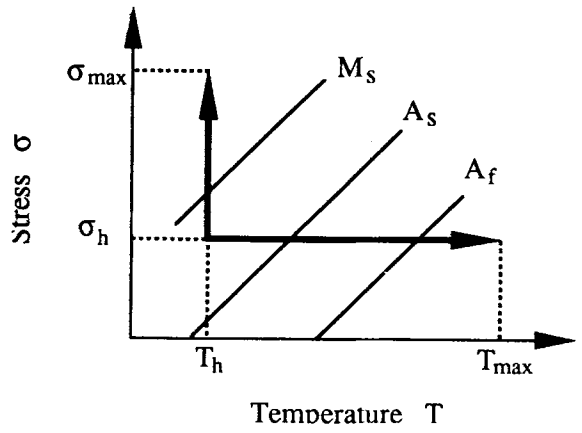

Fig. 2 Schematic of thermomechanical cyclic loading.

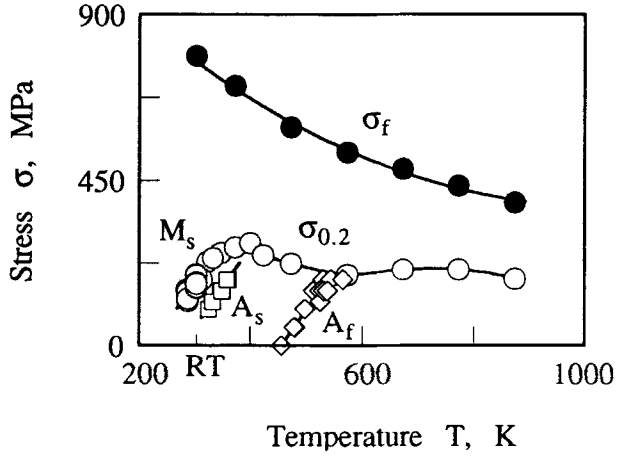

Fig. 3 Transformation lines and temperature dependence of yield stress and tensile strength.

cyclic martensitic/reverse transformations. The M_s^σ point in metallurgy,[12] at which the martensite start line meets the yield stress curve, is about 340 K in this alloy. The M_s line above M_s^σ is discussed below in Section 6 in relation to the plastic deformation in the parent phase.

4. Cyclic Deformation under Free Stress

The thermomechanical hysteretic behavior under free stress, $\sigma_h = 0$ MPa, is illustrated in Fig. 5 at T_h = RT for a constant range of cycling; $\sigma_{max} = 350$ MPa and $T_{max} = 873$ K. Note that the reverse transformation always achieves completion during thermal cycling because $T_{max} > T_{Af} \approx 457$ K under $\sigma_h = 0$ MPa. The martensite start stress σ_{Ms} and the austenite finish temperature T_{Af} measured from the data are plotted versus the number of cycles in Fig. 6 and 7. They do change during cycling, as observed in a Fe-Mn-Si alloy,[13] but very slowly. The austenite start temperature was not able to be clearly determined from the strain-temperature data.

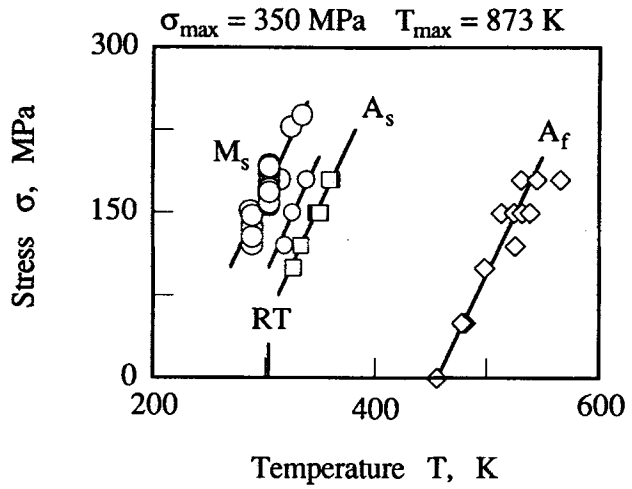

Fig. 4 Transformation lines.

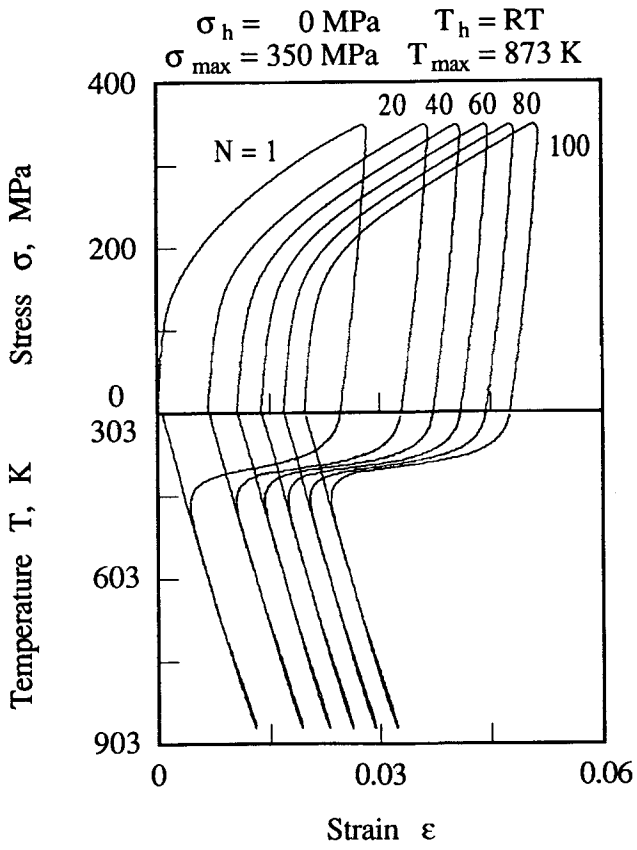

Fig. 5 Thermomechanical hysteresis under free stress.

A certain amount of strain, ε_R illustrated in Fig. 8, remains unrecovered after every thermomechanical cycle, which decreases with the cycle and appears to be reduced finally to a limit value. This means that, contrary to the observation reported by Tobushi et al.[14] in a Ti-Ni alloy, the thermomechanical hysteresis loop never converges to a limit loop, although the

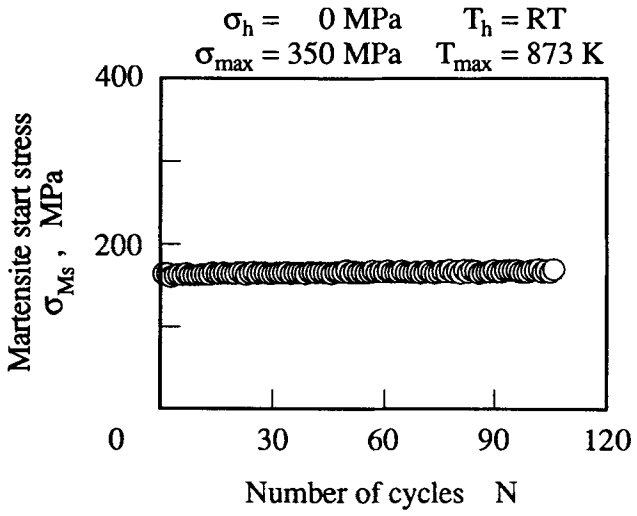

Fig. 6 Change in martensite start stress during cycling.

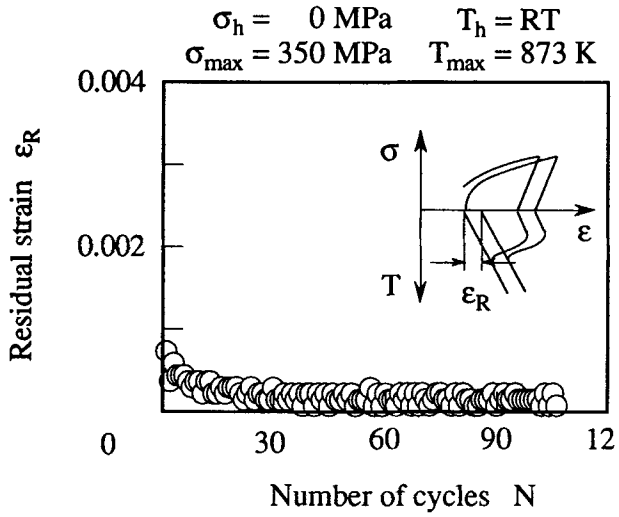

Fig. 8 Change in residual strain during cycling.

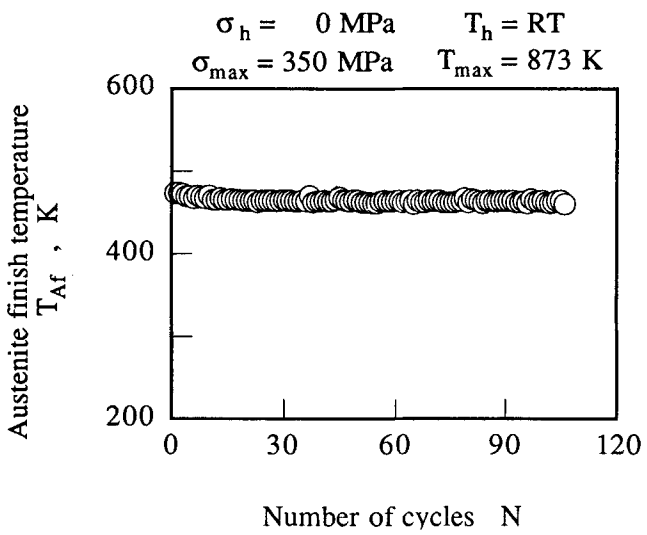

Fig. 7 Change in austenite finish temperature during cycling.

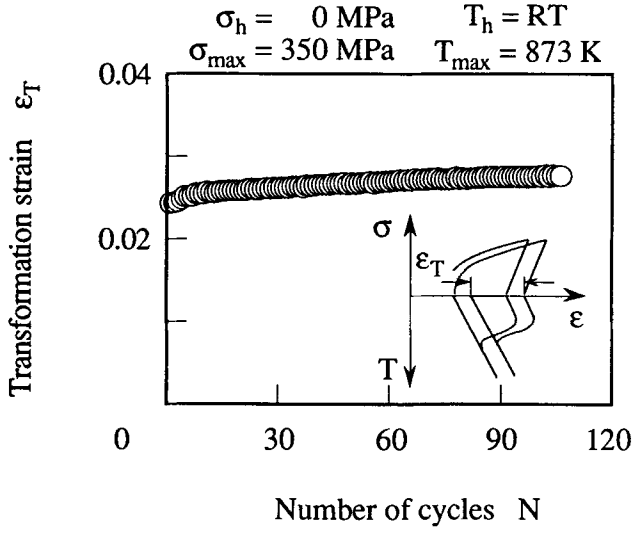

Fig. 9 Change in transformation strain during cycling.

shape of the loop finally tends to a steady form (Fig. 5). The hysteresis loop, from almost 30 cycles of loading on, only shifts cycle by cycle to the higher strain side by an amount $\varepsilon_R \approx 0.005$. The residual strain, ε_R, is understood metallurgically to be induced by dislocations piled continuously in the vicinity of the microscopic defects in the alloy every time the transformation interface passes that point during cycling.[15,16]

The transformation strain, ε_T, defined in Fig. 9, or the strain recovered during the reverse transformation in the thermal run of cycling, increases slowly. The shape recovery in a cycle, which may be estimated from

$$R = \frac{\varepsilon_T}{\varepsilon_R + \varepsilon_T} \times 100\% \qquad [1]$$

exhibits a very high value and increases during cycling, as Fig. 10 illustrates. The full recovery ($R = 100\%$) is, however, not realized because $\varepsilon_R = 0$ is not reached, as clearly observed in Fig. 8.

5. Effect of Hold Stress on Hysteresis

The hysteretic behavior strongly depends on the hold stress, σ_h, as shown in Fig. 11 to 14 for a thermomechanical cycle; T_h = RT, σ_{max} = 350 MPa, T_{max} = 873 K. Note that the thermal branch of cycling during testing was always lower than both the martensite start line and the yield stress $\sigma_{0.2}$ in Fig. 3 and 4, which indicates that no macroscopic plastic deformation progresses in the specimen during testing. The hysteresis loop

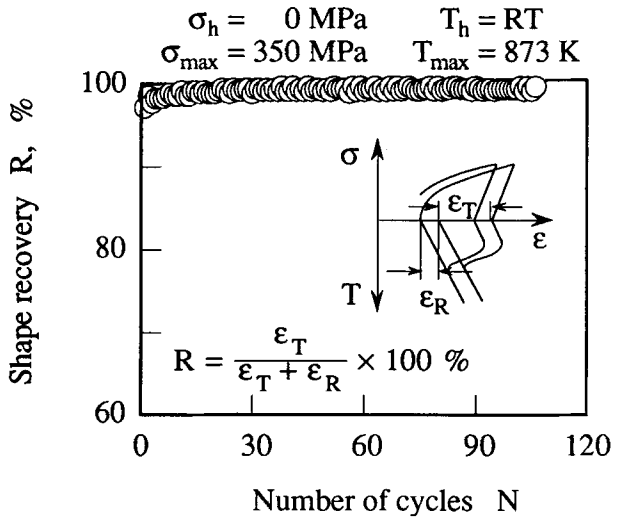

Fig. 10 Change in shape recovery during cycling.

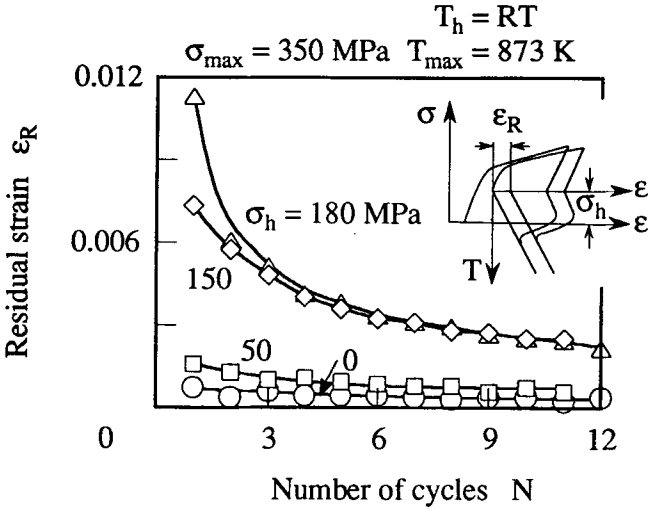

Fig. 12 Effect of hold stress on residual strain.

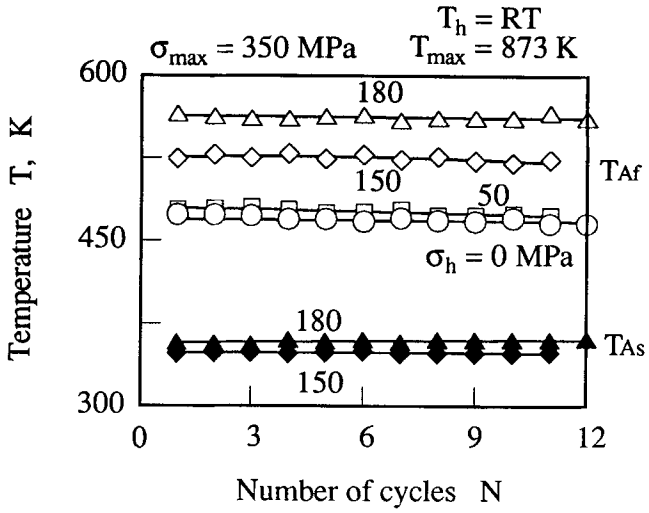

Fig. 11 Effect of hold stress on transformation temperatures.

shifts with the cycle as in the case of free stress discussed in the preceding section. The austenite start temperature, T_{As}, and the austenite finish temperature, T_{Af}, appear almost constant in Fig. 11 within this range of cycling, but are strongly dependent on hold stress. Figure 12 shows that the residual strain ε_R is larger for the higher hold stress, as observed in the Fe-Mn-Si shape memory alloys. The recovery strain, ε_T, on the contrary, is smaller for the larger hold stress during the entire range of cycling considered here, as shown in Fig. 13, which may be explained metallurgically as follows. Plastic deformation almost always progresses microscopically in the vicinity of defects even though the hold stress is far below the macroscopic yield stress, $\sigma_{0.2}$. Of course, the amount is greater under the greater hold stress. This microscopic plastic strain is responsible for the suppression of the full recovery in the heating process. Although the shape recovery increases with the cycle, the value is always lower when the hold stress is higher (Fig. 14).

6. Hysteresis under Imperfect Reverse Transformation

When the thermal branch is cycled under the condition $T_{max} < T_{Af}$, the reverse transformation never reaches completion during heating. The hysteretic behavior appears, therefore, different from those discussed in the preceding sections (Fig. 5, for example). Figures 15 and 16 illustrate the hysteresis loops for T_{max} = 373 and 413 K, respectively, under σ_{max} = 350 MPa, σ_h = 0 MPa, and T_h = RT.

The residual strain after the end of a thermal branch is composed of two parts; the transformation strain, which is fully recoverable if the specimen is heated above T_{Af}, and the irreversible part caused by plastic deformation on the microscopic scale, which is responsible for the change in the hysteresis loops during cyclic loading and is not recovered even if the specimen is heated above T_{Af}.

The hysteresis loop shifts, cycle by cycle to the higher strain side, because a given amount of residual strain always remains after a thermomechanical cycle. The amount of shift per cycle, $\varepsilon_0 - \varepsilon_{rec}$ defined in Fig. 17 and 18, is greater at higher T_{max} values and decreases with the cycle, as in the case of $T_{max} > T_{Af}$.

The more rapid progress of the loops to the higher strain side, compared to the conditions shown in Fig. 5 in which the reverse transformation is completed, can be explained by the fact that the strain recovery is imperfect due to incomplete reverse transformation in the heating process. The amount of strain recovery during thermal loading, ε_{rec}, decreases with the cycle, as shown in Fig. 17 at both temperatures. Figure 18 illustrates that the same is true for the strain range ε_0 during mechanical loading. The shape recovery defined with these strains from

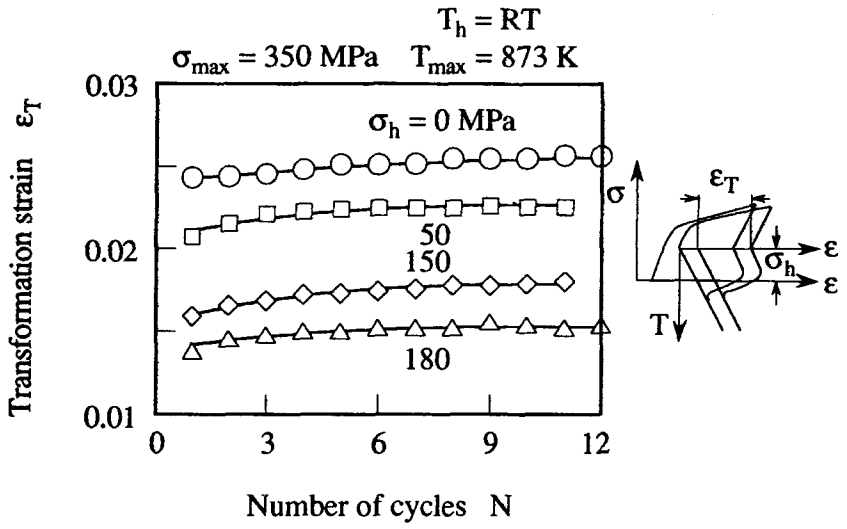

Fig. 13 Effect of hold stress on transformation strain.

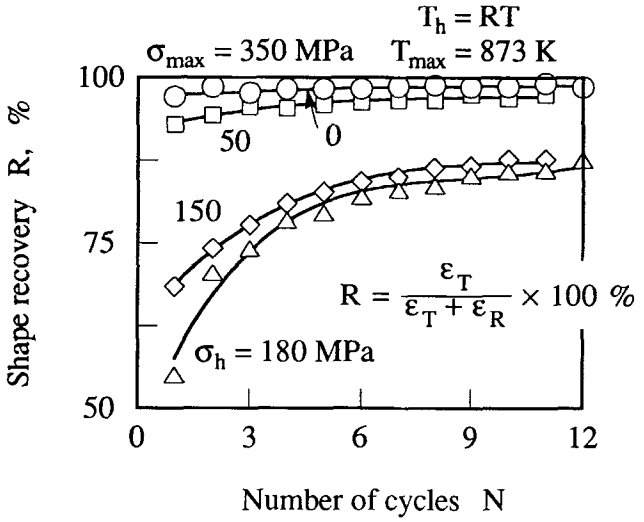

Fig. 14 Effect of hold stress on shape recovery.

$$R = \frac{\varepsilon_{rec}}{\varepsilon_0} \times 100\% \qquad [2]$$

increases with the cycle, as shown in Fig. 19.

In Fig. 15 and 16, the results of the following test conditions are also illustrated. After 14 cycles of thermomechanical loading, the specimen is heated to 873 K and is subsequently cooled to RT, always under free stress. Because the strain-temperature outputs obtained in the thermal branch of the 14th cycle and in

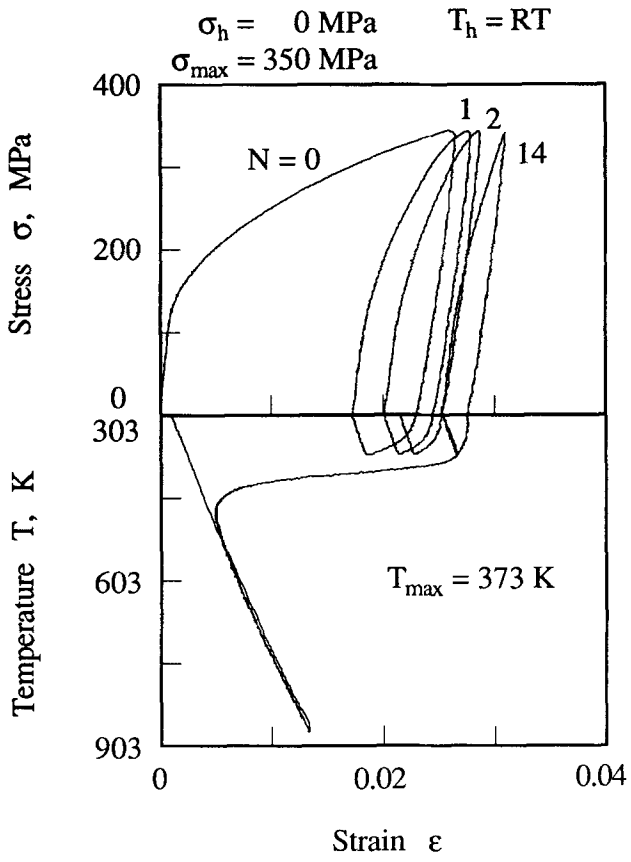

Fig. 15 Hysteresis under imperfect reverse transformation (T_{max} = 373 K).

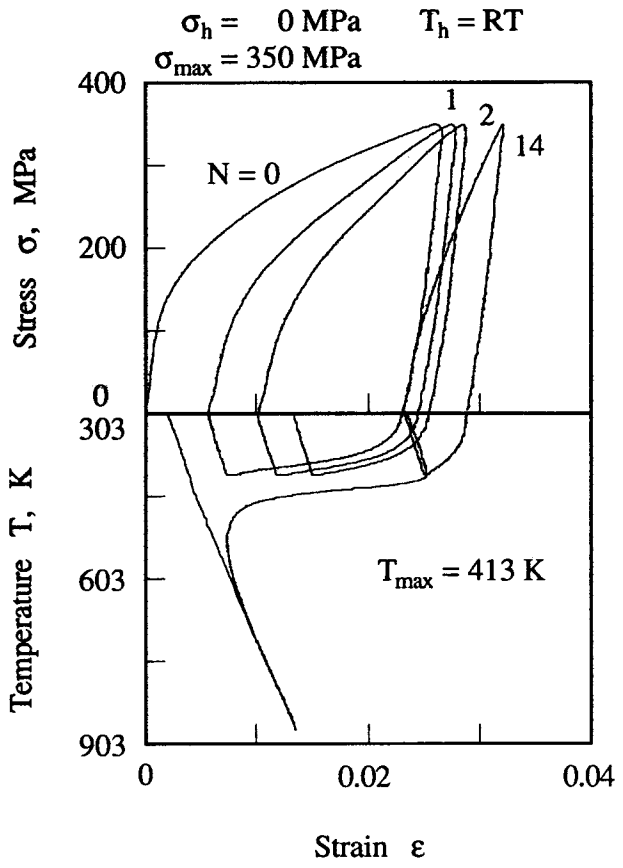

Fig. 16 Hysteresis under imperfect reverse transformation.

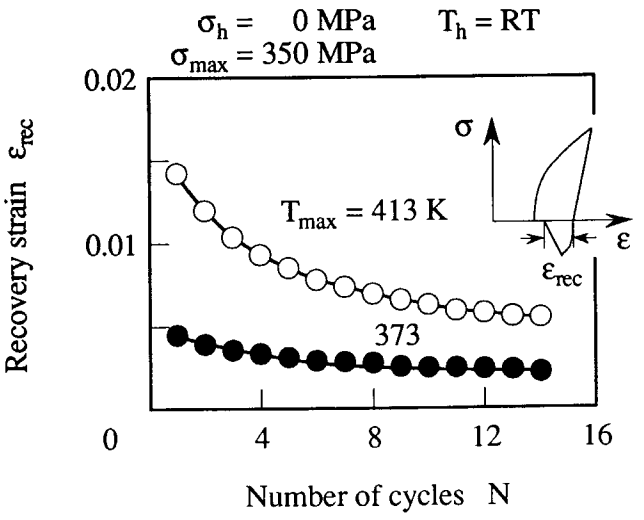

Fig. 17 Recovery strain under imperfect reverse transformation.

the subsequent heating/cooling run constitute a continuous curve and because it fits well to the thermal branch of the 14th cycle in Fig. 5, the complete test results shown in Fig. 15 and 16

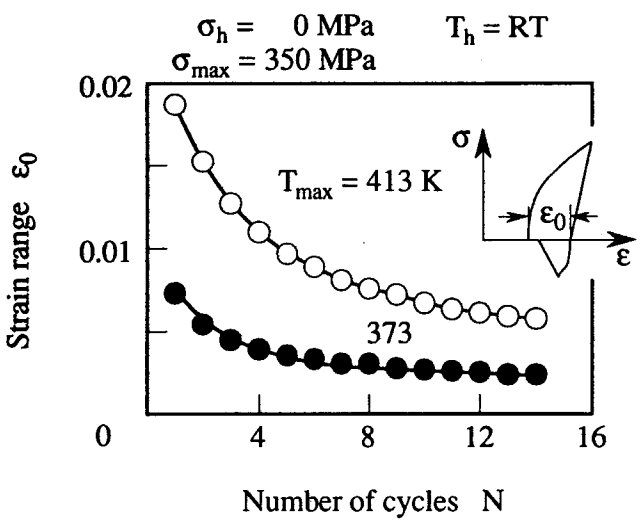

Fig. 18 Strain range under imperfect reverse transformation.

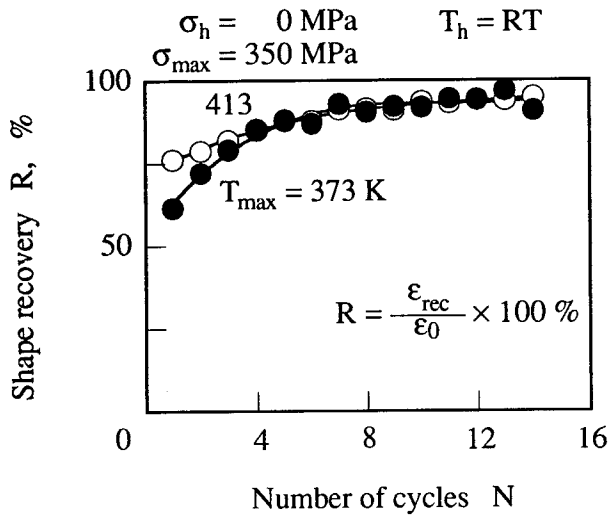

Fig. 19 Shape recovery under imperfect reverse transformation.

can be determined to occur without macroscopic plastic deformation. The residual strain observed after cooling to room temperature is, therefore, solely due to microscopic plastic deformation in the vicinity of microscopic defects. This observation reveals that the different form of hysteresis loops shown in Fig. 15 and 16 is caused by the imperfect reverse transformation, which means that the maximum temperature in the thermal branch of cycling, T_{max}, may be an essential parameter to include in the analysis of the hysteretic phenomena discussed in Sections 3 and 4. Hysteresis finally tends to reach a limiting loop, which is actually two linear lines that consist of an elastic loading/unloading mechanical line and another thermal expansion/contraction thermal line.

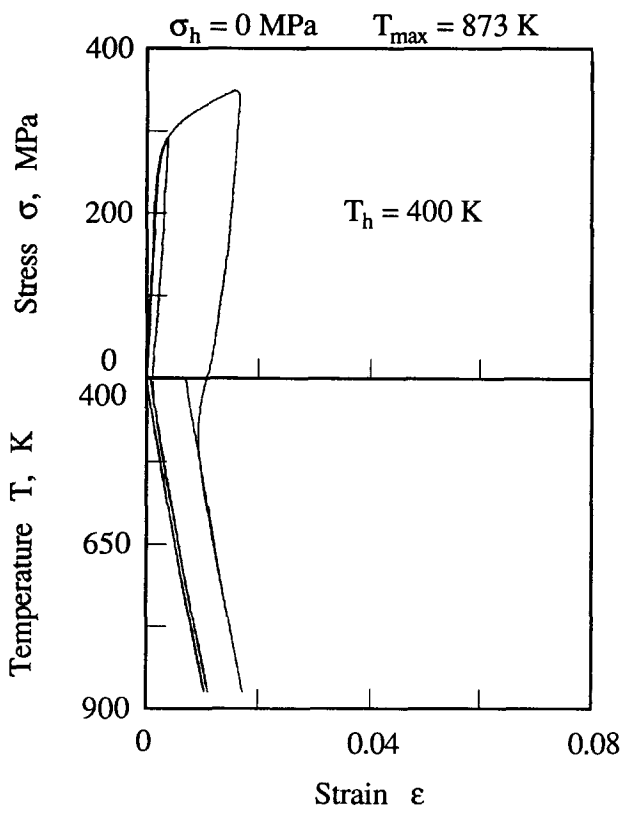

Fig. 20 Thermomechanical hysteresis at T_h = 400 K.

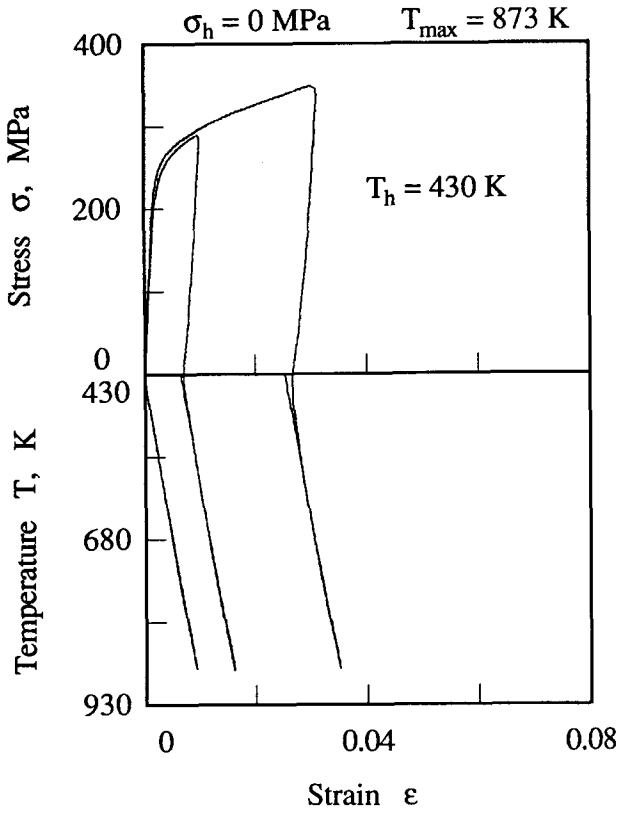

Fig. 21 Thermomechanical hysteresis at T_h = 430 K.

7. Martensite Start Stress Above Yield Stress

Figure 4 shows the martensite start line, at which the martensitic transformation starts, only below the yield stress. If the martensite start line still exists above the yield stress at each temperature level, it indicates that the parent phase undergoes a macroscopic plastic deformation under isothermal loading before the start of the martensitic transformation. The situation is, therefore, exactly the same as in the case of transformation-induced plasticity in steel (TRIP steels).[12]

Figures 20 and 21 illustrate the stress-strain-temperature hysteresis for the first cycle of thermomechanical loading at the different temperature levels; T_h = 400 and 430 K. At each temperature, the mechanical load is applied to 100 MPa, which is far below the yield stress, 290 and 350 MPa, of each test specimen. Figure 20 clearly shows that the loading to 100 MPa at 400 K never triggers the martensite transformation, whereas the hysteresis for loading to 350 MPa strongly suggests the start of the martensitic transformation because a given amount of strain is recovered in the reverse transformation during heating. The curve illustrates that the reverse transformation has already started in the unloading process. The hysteresis for 290 MPa also reveals the strain recovery during heating, although very slightly. A series of tests concludes that the martensite start stress exists between $\sigma_{0.2}$ and 290 MPa at 400 K.

At 430 K in Fig. 21, alloy behavior is elastic under 100 MPa, as is the case at 400 K. However, the alloy clearly exhibits plasticity between $\sigma_{0.2}$ and 290 MPa because no strain recovery is observed during heating. The martensitic transformation most likely starts during loading between 290 and 350 MPa at this temperature. The same conclusion also was obtained at 440 K, and testing at 473 K suggested $\sigma_{Ms} > 350$ MPa.

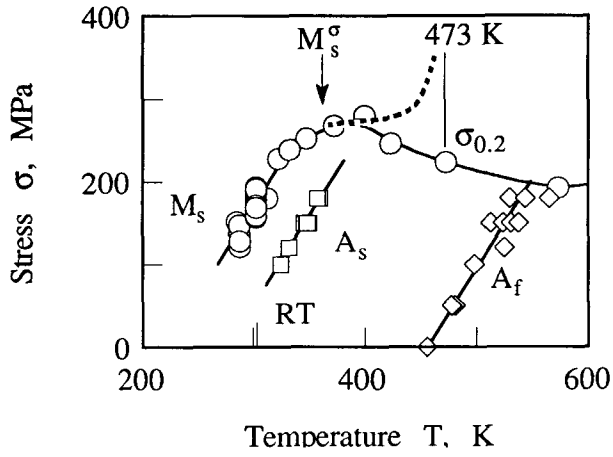

Fig. 22 Martensite start line above M_s^σ point.

Judging from the data obtained to date, the martensite start line above $M_s^\sigma \approx 340$ K must likely be, as shown by the broken line in Fig. 22, above the yield stress. The M_d point in metal-

lurgy, above which no stress-induced martensite is formed, may be around 470 K in this alloy.

Acknowledgments

The early version of this work has been discussed extensively with Prof. C. Lexcellent, Universite de Franche-Comté/France; Prof. F.D. Fischer, Montanuniversität Leoben/Austria; and Prof. B. Buchmayr, Technische Universität Graz/ Austria, when one of the authors (K. Tanaka) visited them individually. He is grateful for the travel grant on those occasions from both the Japan Society for Promotion of Sciences and the Christian Doppler Laboratory for Micromechanics of Materials/Austria. Part of this work was financially supported by the Amada Foundation for Metal Work Technology, as well as by the Grant-in-Aid for Scientific Research (No. 04550093) through the Ministry of Education, Science and Culture, Japan. The authors extend their gratitude to the Steel Research Center/NKK Corporation for supplying the alloy specimens.

References

1. J. Perkins, Ed., *Shape Memory Effects in Alloys*, Plenum Press, 1975
2. H. Funakubo, Ed., *Shape Memory Alloys*, Gordon and Breach Science Publishers, 1987
3. T.W. Duering, K.N. Melton, D. Stöckel, and C.M. Wayman, Ed., *Engineering Aspects of Shape Memory Alloys*, Butterworths-Heinemann, 1990
4. T. Maki and I. Tamura, Shape Memory Effect in Ferrous Alloys, *Proc. ICOMAT-86*, JIM, 1986, p 963-970
5. A. Sato, K. Takagaki, S. Horie, M. Kato, and T. Mori, Cyclic Deformation and Fracture Behavior of Fe-Mn-Si Shape Memory Alloys, *Proc. ICOMAT-86*, JIM, 1986, p 979-984
6. M. Murakami, H. Otsuka, G. Suzuki, and M. Masuda, Complete Shape Memory Effect in Polycrystalline Fe-Mn-Si Alloys, *Proc. ICOMAT-86*, JIM, 1986, p 985-990
7. S. Kajiwara, T. Kikuchi, and N. Sakuma, Shape Memory Effect in High Nickel Steels, *Proc. ICOMAT-86*, JIM, 1986, p 991-996
8. J.H. Yang and C.M. Wayman, Self-Accommodation and Shape Memory Mechanism of ε-Martensite. I. Experimental Observations, *Mater. Charact.*, Vol 28, 1992, p 23-35
9. H. Inagaki, Shape Memory Effect of Fe-14%Mn-6%Si-9%Cr-6%Ni Alloy Polycrystals, *Z. Metallkd.*, Vol 83, 1992, p 90-96, 97-104
10. Y. Moriya, H. Kimura, S. Ishizaki, S. Hashizume, S. Suzuki, H. Suzuki, and T. Sampei, Properties of Fe-Cr-Ni-Mn-Si (Co) Shape Memory Alloys, *J. Phys. IV, Colloque C4, Suppl. J. Phys. III*, Vol 1, 1991, p C4-433/C4-437
11. Y. Moriya, S. Suzuki, S. Hashizume, T. Sampei, and I. Kozaus, Effect of Alloying Elements on Shape Memory Effect of Fe-Cr-Ni-Mn-Si (-Co) Shape Memory Alloys, *Proc. Int. Conf. Stainless Steels*, ISIJ, 1991
12. I. Tamura, Deformation-Induced Martensitic Transformation and Transformation-Induced Plasticity in Steels, *Met. Sci.*, Vol 16, 1982, p 245-253
13. M. Sade, K. Halter, and E. Hornbogen, The Effect of Thermal Cycling on the Transformation Behavior of Fe-Mn-Si Shape Memory Alloys, *Z. Metallkd.*, Vol 79, 1988, p 487-491
14. H. Tobushi, H. Iwanaga, K. Tanaka, T. Hori, and T. Sawada, Deformation Behavior of TiNi Shape Memory Alloys Subjected to Variable Stress and Temperature, *Contin. Mech. Thermodynam.*, Vol 3, 1991, p 79-93
15. S. Miyazaki, T. Imai, Y. Igo, and K. Otsuka, Effect of Cyclic Deformation on the Pseudoelasticity Characteristics of Ti-Ni Alloys, *Metall. Trans. A*, Vol 17, 1986, p 115-120
16. S. Miyazaki and K. Otsuka, Development of Shape Memory Alloys, *ISIJ Int.*, Vol 29, 1989, p 353-377